



EDAP+ TN on Methods and Reference Data for SAR Data Quality Assessments

Author(s): _____ **Andrea Recchia**
Laura Fioretti
Task 3 Team

Approval: _____ **Andrea Recchia**
Task 3 Lead

Accepted: _____ **Clément Albinet**
EDAP+ Technical Officer

AMENDMENT RECORD SHEET

The Amendment Record Sheet below records the history and issue status of this document.

| ISSUE | DATE | REASON |
|-------|------------|--|
| 0.1 | 13/12/2022 | First draft version delivered for EDAP+ SRM #2 |
| 1.0 | 15/03/2023 | First issue of the TN addressing feedback from ESA |
| 1.1 | 17/05/2023 | First issue published on-line |

TABLE OF CONTENTS

| | |
|---|-----------|
| AMENDMENT RECORD SHEET | 2 |
| TABLE OF CONTENTS | 2 |
| 1. EXECUTIVE SUMMARY | 3 |
| 1.1 Applicable Documents..... | 3 |
| 1.2 References..... | 3 |
| 1.3 Glossary..... | 3 |
| 1.4 Introduction | 5 |
| 2. QUALITY ASSESSMENT PROCESS..... | 7 |
| 2.1 Mission quality assessment procedure..... | 7 |
| 2.2 Cal/Val Maturity Matrix | 8 |
| 2.3 Tools for mission quality assessment..... | 9 |
| 3. CALIBRATION SITES | 10 |
| 3.1 Point Target Calibration Sites | 10 |
| 3.2 Rain Forest Distributed Target Sites | 10 |
| 3.3 Low Backscatter Areas..... | 11 |
| 3.4 CEOS Point & Distributed Targets DB | 13 |
| 4. SAR QUALITY MEASURES | 14 |
| 4.1 Products Radiometric Calibration..... | 14 |
| 4.2 Point Target Data Analysis | 15 |
| 4.2.1 Pre-processing..... | 16 |
| 4.2.2 RCS Estimation..... | 16 |
| 4.2.3 Range and Azimuth resolution..... | 17 |
| 4.2.4 Side Lobe Levels | 18 |
| 4.2.5 Point Targets localization | 21 |
| 4.3 Distributed Target Data Analysis..... | 22 |
| 4.3.1 Beta/Sigma/Gamma-Zero profiles | 22 |
| 4.3.2 Beam-to-beam calibration and EAP compensation | 25 |
| 4.3.3 Azimuth scalloping | 25 |
| 4.3.4 NESZ level..... | 26 |
| 4.3.5 Equivalent Number of Looks (ENL) | 28 |

1. EXECUTIVE SUMMARY

This technical note represents D-7 in the framework of EDAP+. It is intended as a reference document providing details of methods applied and reference sites exploited for the quality assessments of SAR data.

1.1 Applicable Documents

The following is a list of applicable documents with a direct bearing on the content of this report. Where referenced in the text, these are identified as [AD-n], where 'n' is the number in the list below:

- AD-1. EDAP Statement of Work, ESA-EOPG-EOPGMQ-SOW-39, Issue 1 Rev 1, 14/12/21

1.2 References

The following is a list of reference documents with a direct bearing on the content of this report. Where referenced in the text, these are identified as [RD-n], where 'n' is the number in the list below:

- RD-1. EDAP Best Practice Guidelines, EDAP.REP.001, v1.2, September 2019.
- RD-2. S. N. Madsen, Estimating the Doppler Centroid of SAR Data, *IEEE Transactions on aerospace and electronic systems*, vol. aes-25, no. 2, March 1989
- RD-3. D. Small, Flattening Gamma: Radiometric Terrain Correction for SAR Imagery, in *IEEE Transactions on Geoscience and Remote Sensing*, vol. 49, no. 8, pp. 3081-3093, Aug. 2011, doi: 10.1109/TGRS.2011.2120616.
- RD-4. https://eo4society.esa.int/wp-content/uploads/2021/02/D1T1b_LTC2015_Younis.pdf
- RD-5. https://ccrma.stanford.edu/~jos/sasp/Hamming_Window.html

1.3 Glossary

The following acronyms and abbreviations have been used in this document.

| | |
|------|---|
| CEOS | Committee on Earth Observation Satellites |
| DC | Doppler Centroid |
| DEM | Digital Elevation Model |
| EAP | Elevation Antenna Patterns |
| ECEF | Earth Centered Earth Fixed |
| ENL | Equivalent Number of Looks |
| ESA | European Space Agency |
| IRF | Impulse Response Function |
| ISLR | Integrated Side Lobe Ratio |
| LOS | Line Of Sight |



| | |
|------|-----------------------------------|
| NESZ | Noise Equivalent Sigma Zero |
| PSLR | Peak Side Lobe Ratio |
| PT | Point Target |
| QAP | Quality Assessment Process |
| RCS | Radar Cross Section |
| RF | Rain Forest |
| SAR | Synthetic Aperture Radar |
| SCT | SAR Calibration Toolbox |
| SLC | Single Look Complex |
| SNCR | Signal to Noise and Clutter Ratio |
| SQT | SAR Quality Toolbox |

1.4 Introduction

In this document, several aspects of the SAR data quality assessment process are touched upon, starting from the process steps and then providing details on the reference calibration sites that can be exploited as well as on the methods that are applied for the assessment of quality parameters.

The whole Quality Assessment Process (**QAP**), including preliminary steps and interactions with the mission responsible and European Space Agency (**ESA**) responsible, is pictorially reported in the flowchart below.

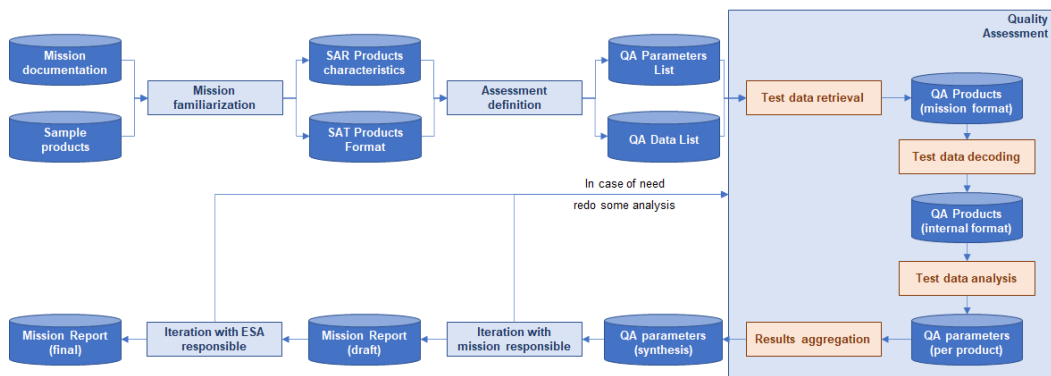


Figure 1-1: High level flowchart of the Quality Assessment Process

For the quality assessment, which includes analyses of radiometric and polarimetric calibration, Impulse Response Function (**IRF**) quality as well as geometric accuracy, a series of calibration sites with specific conditions, should be exploited. Those sites include:

- **Point Target (PT) calibration sites** (preferably including both corner reflectors and transponders), for the assessment of the absolute radiometric and polarimetric calibration, for the IRF quality and for the geometric accuracy.
- **Rain forest distributed target sites**, for the relative radiometric calibration and antenna pattern correction assessment.
- **Low backscatter areas**, for the assessment of the noise level.

The quality parameters, to be measured and compared against product specifications, which are identified as an optimal set for the quality assessment of SAR data are reported in **Table 1-1** below.

Table 1-1: Parameters for the assessment of SAR data quality

| Quality parameter | Metric | Data type | Cal. Sites |
|-------------------|---|---------------------------------|--|
| IRF | Spatial resolution | Point Target | Mission dedicated sites: Rosamond Corner Reflector Array (California) Surat Basin (Australia) |
| | Peak-to-Side Lobe ratio | Point Target | |
| | Integrated Side Lobe ratio | Point Target | |
| Geometry | Localization | Point Target | |
| Radiometry | Calibration constant | Point Target | |
| | Polarimetric imbalance | Point Target | |
| | Elevation Antenna Pattern | Rain Forest | Amazon, Congo Sahara Greenland |
| | Azimuth scalloping | Rain Forest | |
| | Beam-to-beam offset | Rain Forest | |
| | Equivalent Number of Looks (ENL) | Rain Forest, Desert, Ice Sheets | |
| | Noise level | Low backscatter | Calm sea areas (e.g., Doldrums) Lakes (for small swaths, e.g., Mono Lake - California) Deserts |

2. QUALITY ASSESSMENT PROCESS

2.1 Mission quality assessment procedure

The whole quality assessment process, already introduced in **Figure 1-1**, can be summarized in the following steps:

1. **Mission familiarization:** the documentation on the SAR mission (website of the mission, product specification and format documents, user guides) to be assessed is collected and analyzed in order to identify the main characteristics of the products to be assessed. At this stage, in cooperation with mission responsible/representatives, a few sample products are also collected to start the implementation of the tools needed for the management of the mission SAR products in the analysis tools.
2. **Assessment definition:** based on the output of the first step, the list of parameters to be measured (that could be a sub-set of those reported in **Table 1-1**) and a set of products required to perform the mission assessment are defined. The definition of the set of products to be analyzed is carried out in cooperation with the entity operating the mission (e.g., based on the mission acquisition plan).
3. **Quality assessment:** the SAR products identified at the previous step are retrieved and analyzed to derive the SAR quality parameters defined for the considered mission.
4. **Iteration with mission responsible:** based on the outcome of the quality assessment, an iteration with the entity operating the mission is performed to address any potential open points (e.g., discrepancies between measured and product specification values). As an outcome of this iteration, the analysis of additional products could be required.
5. **Iteration with ESA responsible:** the final report on the mission quality is prepared based on the results collected during the execution of the previous steps. A first issue of the document is provided to ESA and to the data provider for review and, based on the received feedback, the final version is prepared before publication on the EDAP website.

Step 3 (quality assessment), representing the core activity of the whole process, can be further detailed as follows:

- 3.a. **Test data retrieval:** the agreed set of SAR products is retrieved either through direct exchange with the mission responsible or through the standard data access platform for the mission data users. The second option (that is sometimes unfeasible depending on the mission) is preferred, since it allows to assess the mission data procurement procedure. At this stage, the final check on the suitability of the identified products for the QAP is performed. Sample suitability checks that are performed include: the conformity of the data to products specification (e.g., the ground coverage, the polarimetric channels, etc.), the presence of evident artifacts that could impair the assessment, the visibility of calibration targets (for acquisitions over the calibration sites) or the presence of rivers or other natural features (for acquisitions over distributed targets calibration sites).
- 3.b. **Test data decoding:** the SAR products that pass the first suitability check are ingested in the SAR data analysis tools to perform the required analyses. SAR products are usually made of a set binary file (e.g., in Geo tiff format) including the SAR measurements and a set of text files (e.g., in xml format) reporting all the metadata required to interpret the SAR measures. The tools developed for the ingestion of the mission products allow to extract the relevant parameters from the metadata and to extract portion of SAR data from the binary files. During the process, it is possible to detect further issues in the retrieved SAR products (e.g., format or content issues).

3.c. **Test data analysis:** the SAR products are finally analysed to retrieve the mission specific quality parameters. Further details on the performed analyses are reported in the following sections.

3.d. **Results aggregation:** the last step consists of the synthesis of the results collected over the analysed products. Statistical outliers are discarded, and quality parameters are defined averaging the achieved results. Finally, plots representing the overall assessment results and tables with the collected statistics are produced. The produced plots and tables will become the core of the Mission Quality Assessment Report.

2.2 Cal/Val Maturity Matrix

The Mission Quality Assessment Report including all the results of the performed activities is finally generated after necessary iterations with the entity responsible for the mission and with ESA. In particular, the Summary Cal/Val Maturity Matrix and Validation Cal/Val Maturity Matrix, as reported in Figure 2-1 and Figure 2-2, are included in the report. For further details on the maturity matrices please see [RD-1].























| Data Provider Documentation Review | | | Validation Summary | Key |
|--|--|---|---|--|
| Product Information | Metrology | Product Generation | | Not Assessed |
| Product Details  | Sensor Calibration & Characterisation  | Calibration Algorithm  | Measurement Validation Method  | Not Assessable |
| Availability & Accessibility  | Geometric Calibration & Characterisation  | Geometric Processing  | Measurement Validation Results Compliance  | Basic |
| Product Format, Flags & Metadata  | Metrological Traceability Documentation  | Retrieval Algorithm  | Geometric Validation Method  | Good |
| User Documentation  | Uncertainty Characterisation  | Mission-Specific Processing  | Geometric Validation Results Compliance  | Excellent |
| Ancillary Data  | | | | Ideal |
| | | | |  Not Public |

Figure 2-1: Summary Cal/Val Maturity Matrix

| <Entity> Detailed Validation | | | |
|---|---|---|---|
| Measurement | | Geometric | |
| Measurement Validation Activity #1 Method  | Measurement Validation Activity #1 Results Compliance  | Geometric Validation Activity #1 Method  | Geometric Validation Activity #1 Results Compliance  |
| ... | ... | ... | ... |


| Key |
|--|
| Not Assessed |
| Not Assessable |
| Basic |
| Good |
| Excellent |
| Ideal |
|  Not Public |

Figure 2-2: Validation Cal/Val Maturity Matrix

2.3 Tools for mission quality assessment

The mission quality assessment has been performed so far with the following procedure:

1. Download of the products to analyze.
2. Conversion of the products into an internal format that can be managed by proprietary analysis tools developed by Aresys (called Sar Quality Toolbox, **SQT**).
3. Analysis of the data with the SQT and generation of the quality reports.

One of the goals of EDAP+ project is to provide a set of open-source tools that can be used to independently repeat the analyses reported in the EDAP technical notes. The idea is that the open-source tool will be python based and hosted on a public GitHub repository so that users will be able to contribute to analysis tools. The open-source tool will be developed starting from the Sar Calibration Tool (**SCT**) that has been developed to assess the geolocation accuracy of Sentinel-1 products. The **SCT** tool is available at the following link:

<https://github.com/aresys-srl/sar-calibration-tool>

3. CALIBRATION SITES

For the SAR data quality assessment, a series of calibration sites with specific conditions, can be exploited.

3.1 Point Target Calibration Sites

Point target calibration sites can be exploited for the assessment of the absolute radiometric and polarimetric calibration, for the IRF quality and for the geometric accuracy. External calibration is performed by the deployment of reference targets that must be characterized in terms of:

- Radar Cross Section (**RCS**) (related to the size and shape of the reflector)
- Position and orientation

In particular, corner reflectors are used to measure geolocation accuracy of SAR products, they are particularly well suited for this kind of assessment since, contrary to transponders, do not introduce any instrument delay. On the other hand, transponders, which are more easily characterizable in terms of RCS with respect to the corner reflectors, are more commonly used for the absolute calibration of SAR products.

As an example, the corner reflectors in Rosamond calibration site, located in California, are pictorially represented in **Figure 3-1**.



Figure 3-1: Corner reflectors in Rosamond calibration site, California

3.2 Rain Forest Distributed Target Sites

Rain Forest (**RF**) is a natural calibration site for SAR missions due to the homogeneity of the scene. The γ^0 -profiles derived from acquisitions over those areas are assumed to be flat and thus can be exploited to verify the Elevation Antenna Patterns (**EAP**) compensation and beam-to-beam radiometric offsets.

Typical areas in which this characteristic can be observed are for example the Amazon rain forest and the Congo rain forest, which are pictorially represented by **Figure 3-2**.

The approximated boundaries of these calibration sites are reported in **Table 3-1**.



Figure 3-2: Rain Forest areas

Table 3-1 Boundaries of the Rain Forest calibration sites

| Region | NW Latitude [deg] | NW Longitude [deg] | SE Latitude [deg] | SE Longitude [deg] |
|--------------------|-------------------|--------------------|-------------------|--------------------|
| Amazon Rain Forest | -4,99 | -70,54 | -9,13 | -65,67 |
| Congo Rain Forest | 3,60 | 21,44 | -2,64 | 29,26 |

3.3 Low Backscatter Areas

Those regions and areas in which the backscatter level is particularly low can be exploited for measuring the Noise Equivalent Sigma Zero (**NESZ**) directly from Single Look Complex (**SLC**) data.

Those particular conditions can be found in calm waters or deserts as for example the oceanic areas of the Doldrum, a belt close to the equator in which the winds are particularly low and the water very calm. For smaller acquisitions other areas are well suited for the NESZ measurement, such as the Mono Lake in California. Examples of acquisitions over those two mentioned areas are reported in **Figure 3-3** and **Figure 3-4**.

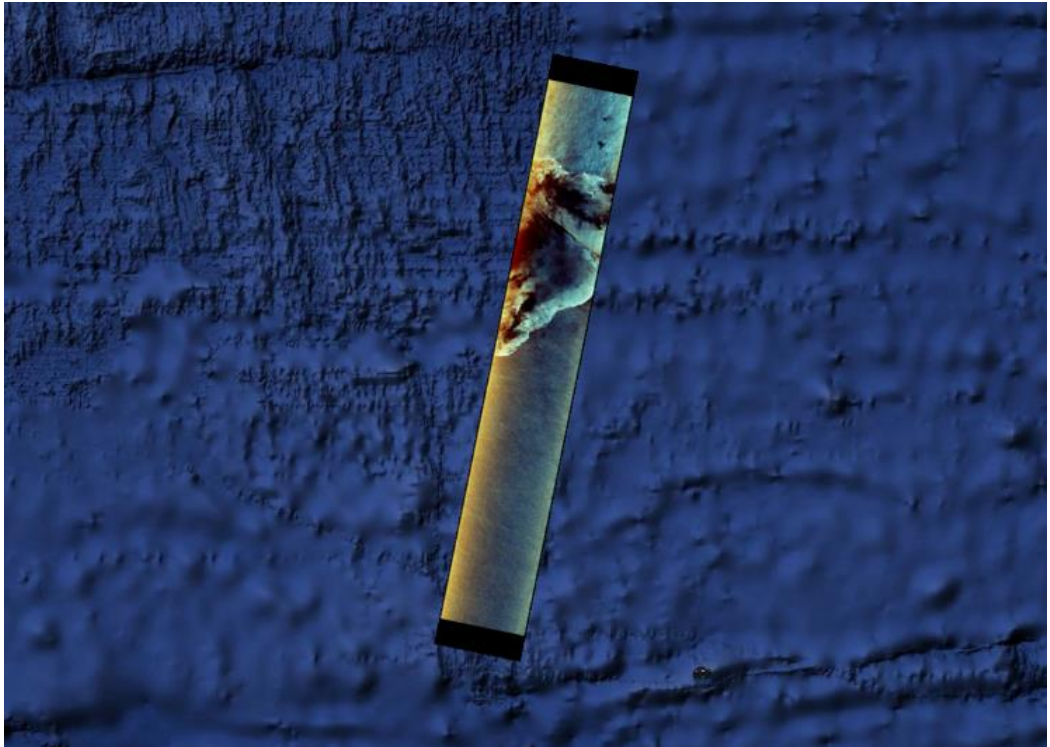


Figure 3-3: Acquisition over Doldrums in the Atlantic Ocean

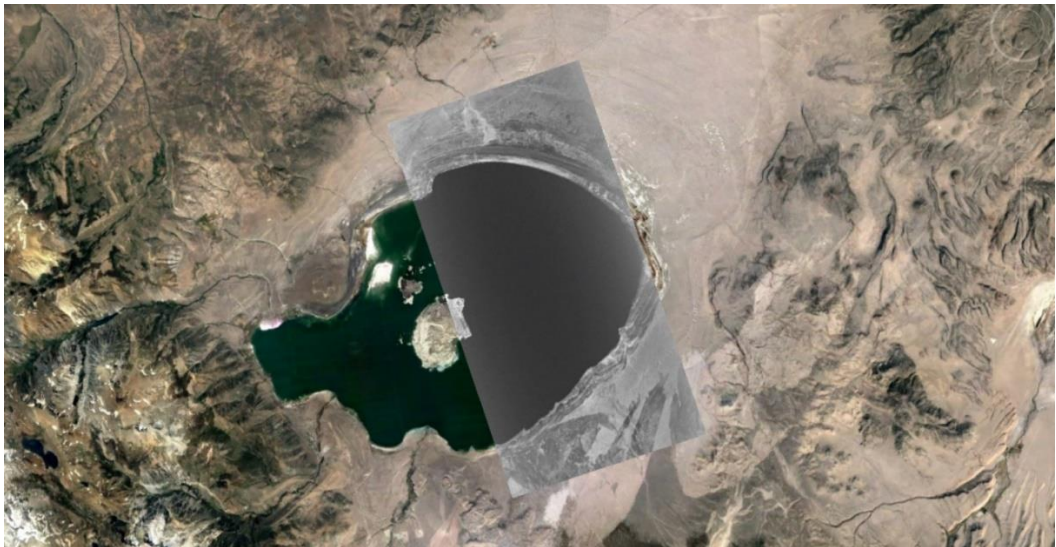


Figure 3-4: Acquisition over Mono Lake, California

3.4 CEOS Point & Distributed Targets DB

One of the objectives of the Committee on Earth Observation Satellites (**CEOS**, <https://ceos.org/>), and of the SAR Subgroup in particular, is the interchange on calibration sites and targets. A data base of calibration sites, including some of those exploited for EDAP+ mission quality assessment, can be found at the following link:

<https://calvalportal.ceos.org/point-distributed-targets-db>

4. SAR QUALITY MEASURES

In the following sections, the methods for the assessment of the quality parameters introduced in **Table 1-1** are presented.

4.1 Products Radiometric Calibration

Before introducing the algorithms, it is useful to recall the radiometric calibration corrections performed at processing level. The radiometric corrections are applied after focusing impact on the relative and absolute radiometric accuracy and are aimed at compensating all the gain factors that depend on the instrument, the propagation and the scene observation geometry. **Figure 4-1** provides a flow chart with the typical radiometric calibration corrections applied to focused SAR data.

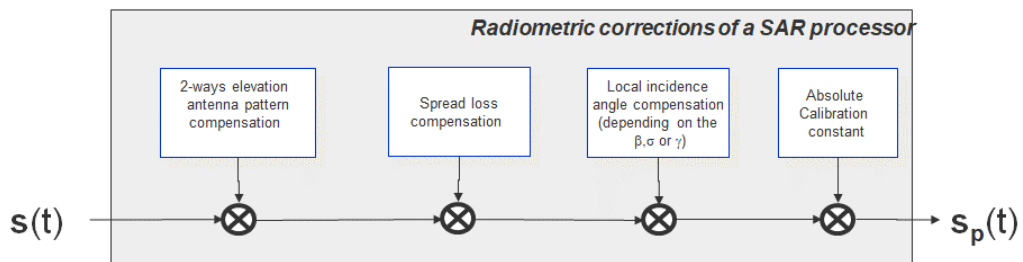


Figure 4-1: Radiometric corrections applied on focused data

The main radiometric corrections include:

- 2-ways elevation antenna pattern
- Spread losses
- Local incidence angle or local radar backscattering area [RD-3]
- Absolute calibration constant

The 2-way elevation antenna pattern correction compensates for the range variant gain of the radar antenna. Two key elements are needed: the gain variation of the antenna pattern with respect to observation angle and the observation angle itself to be derived from the observation geometry. Inaccuracies in the knowledge of the antenna pattern or of the observation geometry can lead to radiometric artefacts in the SAR data.

The spreading losses compensation is aimed at compensating for the power decay induced in the image by the spherical waves' propagation. This term is proportional to the third power of the slant range and can be compensated with great accuracy since the target distance is well known.

The local incidence angle compensation is aimed at compensating for the radiometric distortions introduced by the observation geometry of the targets on ground. The compensation is based on the local incidence angle that can be calculated using either an ellipsoid Earth model (e.g. WGS84) or a Digital Elevation Model (**DEM**) of the scene. The second method provides more accurate results at the cost of a greater computational cost.

The incidence angle compensation is not needed for points targets whose RCS is independent on the resolution cell size, but is fundamental for distributed targets whose

RCS depends on the area of the resolution cell. The compensation of the incidence angle is indeed aimed at compensating for the variations of the resolution cell area within the SAR image due to observation geometry [RD-3]. A resume of the applied corrections is provided in **Table 4-2**.

The last correction step is the application of the absolute calibration constant to convert pixel values from float numbers to the radar quantities described above. The calibration constant is usually derived during the Commissioning Phase of a SAR mission.

4.2 Point Target Data Analysis

The images with strong point targets standing out from the background can be exploited to verify the properties of the 2D IRF. The properties that can be measured from point target data include:

- RCS for absolute and polarimetric calibration
- Spatial resolution
- Side lobe levels
- Localization

The comparison of the measured values with the ones for the system design allow to verify that the data processing is correctly performed and the data quality is nominal. The following figure shows an example of a point target IRF observed in a SAR product.

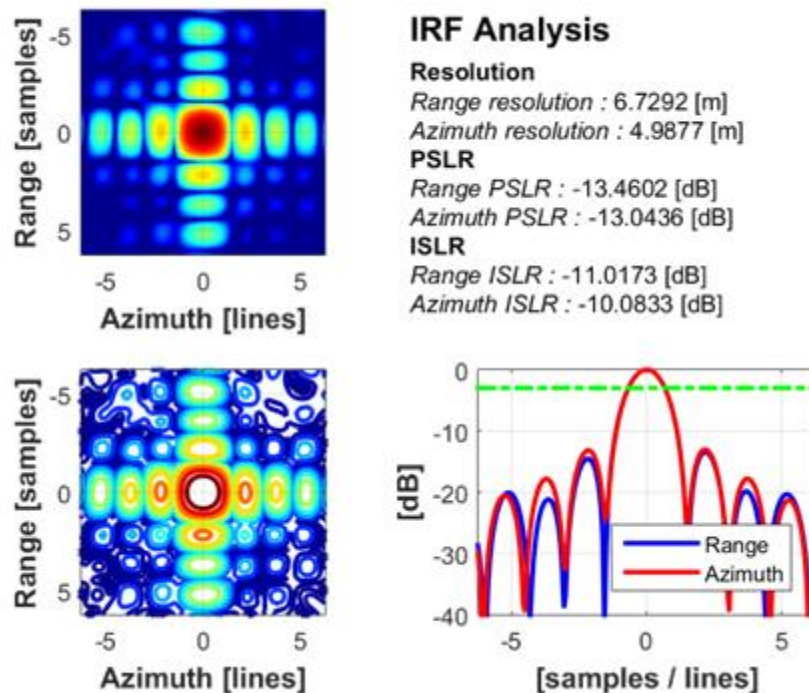


Figure 4-2: Example of point target IRF from a SAR product

4.2.1 Pre-processing

The analysis of point target data is based on two pre-processing steps aimed at improving the quality of the estimated calibration parameters:

1. Identification of the point target within the SAR image
2. 2D oversampling of the area of the image where the point target is located

The first step can be performed either automatically (if the position of the target is known in advance) or manually by visual inspection of the SAR image. It is important to note that not all the point targets are suitable for quality verification. The selected point targets shall be isolated (ideally more than 20 resolution cells) to avoid mutual interference and brighter than the background clutter (ideally more than 20 dB above). The second step is achieved by performing an ideal interpolation of the data in the spectral domain. A typical interpolation factor of 8 or 16 is usually considered for this operation.

The obtained oversampled image includes, at the center, the point target and can be segmented as represented in **Figure 4-3**, where the colours represent the different areas of the image where the different point target IRF parameters will be estimated.

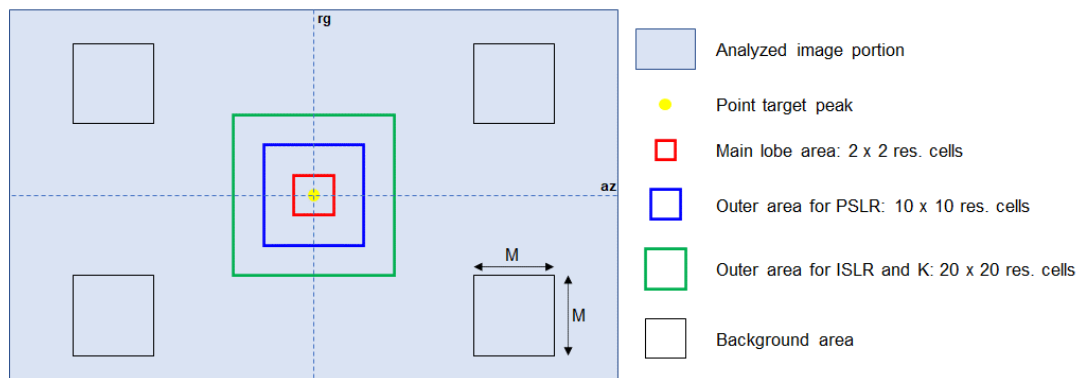


Figure 4-3: Point target image segmentation for IRF analysis

4.2.2 RCS Estimation

The estimation of the RCS of a point target from a SAR image is aimed at the assessment/derivation of the absolute radiometric calibration and polarimetric co-registration of the SAR product. The RCS estimation process foresees the measurement of the energy falling within the main lobe of the focused point target and the removal of the background energy estimated in image regions outside the 2D IRF. The input data shall be provided in β^0 with no incidence angle compensation applied.

Making reference to **Figure 4-3**, the following processing steps are performed on the oversampled image including the point target IRF:

1. Conversion of pixel values to intensity:

$$I(Rg; Az) = |SLC(Rg, Az)|^2$$

2. Derivation of the background intensity I_{BG} by averaging the pixel intensities over four square areas of M pixels (e.g. M = 15) positioned around the target in such a way that they include only clutter intensity.

3. Subtraction of the mean background intensity from the image:

$$I_c(Rg; Az) = I(Rg; Az) - I_{BG}$$

4. Estimation of the RCS of the point target by integrating (summing) the intensity over the pixels belonging to the main lobe of the IRF (red square in **Figure 4-3**) multiplied by the pixel area P_A in the slant range plane.

$$I_p = \sum_{Peak} I_c(Rg; Az) P_A$$

Note that the background intensity estimation can also be performed over the non-oversampled data since its accuracy only depends on the independent pixels considered. The algorithm returns both the target RCS and the background intensity. The ratio between the two values defines the Signal to Noise and Clutter Ratio (**SNCR**). The higher the SNCR the more accurate the estimated target RCS.

Computing the difference between the measured RCS of a well-characterized known target and its real RCS allows to perform the absolute radiometric calibration. The channel distortion, i.e., the difference in a corner reflector RCS between two polarizations, is also measured.

4.2.3 Range and Azimuth resolution

The SAR resolution in the azimuth (along-track) and range (cross-track) directions is defined as the -3 dB lobe width of the 2D IRF sections intersecting at IRF peak. Making reference to **Figure 4-3**, the two directions are represented by the dash-dot lines intersecting at the center of the image. The theoretical resolution can be predicted from the processing parameter of the products according to [RD-4]:

$$RgRes_{Theo} = 0.886 \times \frac{c}{2 \cdot B_{Rg}} \alpha_{Win,rg} \quad (1)$$

$$AzRes_{Theo} = 0.886 \times \frac{v_{sat,grd}}{B_{Az}} \alpha_{Win,az} \quad (2)$$

where c is the speed of light B_{Rg} is the transmitted pulse bandwidth, $v_{sat,grd}$ is the platform velocity projected on ground, B_{Az} is the processed azimuth bandwidth and $\alpha_{Win,rg}$ and $\alpha_{Win,az}$ are the IRF broadening factors corresponding to the Hamming spectral weighting used for side lobe levels reduction [RD-5]. The term 0.886 accounts for the fact that resolution is measured at -3 dB of the IRF and not at the first 0. The following table provides the expected IRF broadening factor associated to different Hamming window coefficients. The expected side lobe levels (see next sections) are also provided.

Table 4-1 IRF broadening factor associated side lobe levels for different hamming window parameters

| Hamming Window Coefficient | IRF Broadening Factor | Peak Side Lobe Ratio (PSLR) [dB] | Integrated Side Lobe Ratio (ISLR) [dB] |
|----------------------------|-----------------------|----------------------------------|--|
| 0.5 | 1,63 | -31,47 | -32,88 |
| 0.6 | 1,32 | -31,60 | -26,18 |
| 0.7 | 1,18 | -24,07 | -19,10 |
| 0.8 | 1,09 | -18,65 | -14,87 |
| 0.9 | 1,04 | -15,34 | -12,14 |

| | | | |
|---|------|--------|--------|
| 1 | 1,00 | -13,26 | -10,21 |
|---|------|--------|--------|

The theoretical resolution values can be compared against the resolution measured from the data. The input is the oversampled image around the point target location as represented in **Figure 4-4**. The profiles along range (top plot on the right) and azimuth (bottom plot on the right) directions are then extracted and the 3 dB lobe width in pixels ΔPix_{-3dB} is measured from the profiles. The measured width can then be converted into resolution values according to the following relationships:

$$RgRes_{data} = \Delta Pix_{-3dB} \cdot \frac{c}{2 \cdot f_{s,Rg}} \quad (3)$$

$$AzRes_{data} = \Delta Pix_{-3dB} \cdot \frac{v_{Sat,grd}}{f_{s,Az}} \quad (4)$$

where $f_{s,Rg}$ and $f_{s,Az}$ are the sampling frequencies along range and azimuth axes. The measured resolution can then be compared against the theoretical values reported in (1) and (2). A measured resolution higher than the theoretical one can be an indicator of some issue at processing level (e.g. inaccurate orbit information available).

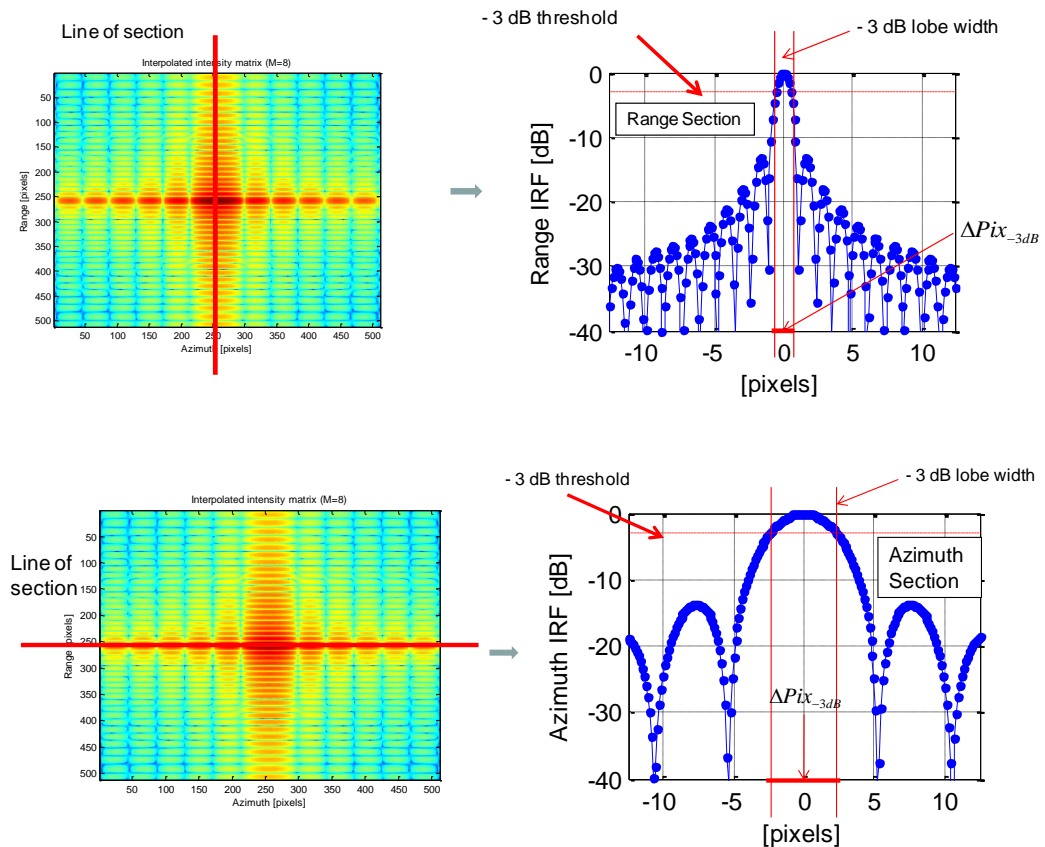


Figure 4-4: Examples of resolution's measurements on point target. Upper panel: range measurement. Lower panel: azimuth measurement.

4.2.4 Side Lobe Levels

The side lobe levels control is a fundamental step of SAR processing implemented, as discussed in the previous section, applying a Hamming window to the range and azimuth

spectra. According to the Hamming window parameter selected for the SAR data under analysis, a particular level of the side lobes is expected as reported in **Table 4-1**.

Regardless of the azimuth/range section, the side lobe levels can be expressed as:

- Peak to Side Lobe Ratio (PSLR) defined as the ratio between the maximum in both peak area and side lobes area. It is a measure of the contrast (i.e., the capability of distinguish two adjacent PTs) or of the blurring of the PT, since it measures leakage of main lobe energy into side lobes.
- Integrated Side Lobe Ratio (ISLR) is defined as the ratio between the integrated intensity in both peak area and side lobes area. It measures the energy associated with the main lobe with regards to the energy of the side lobes. The ratio gives the measurement of how much energy is inside lobe instead of main lobe.

Making reference to **Figure 4-3**, the two areas for the PSLR and ISLR measurement are represented by the blue and green lines respectively. The below formula provides an example of the process to be performed for the measurement of the PSLR from the range and azimuth profiles extracted from the 2D oversampled image. The peak of the main lobe is measured in the red area corresponding to two resolution cells around the peak location. The peak of the side lobes is measured within the green area corresponding to 4 resolution cells to the left and to the right of the main lobe. The PSLR value is then readily obtained according to:

$$PSLR = -10 \cdot \log_{10} \left(\frac{\max \{ S_{PeakArea} \}^2}{\max \{ S_{SideArea} \}^2} \right) \quad (5)$$

where:

$$-Res < PeakArea < Res$$

$$\{-5 \times Res < SideArea < -Res\} \cup \{Res < SideArea < 5 \times Res\}$$

The PSLR can be measured separately for range and azimuth IRF, given that usually different Hamming windows are used in processing. The PSLR definition can be extended to the 2D by taking the 1D worst case.

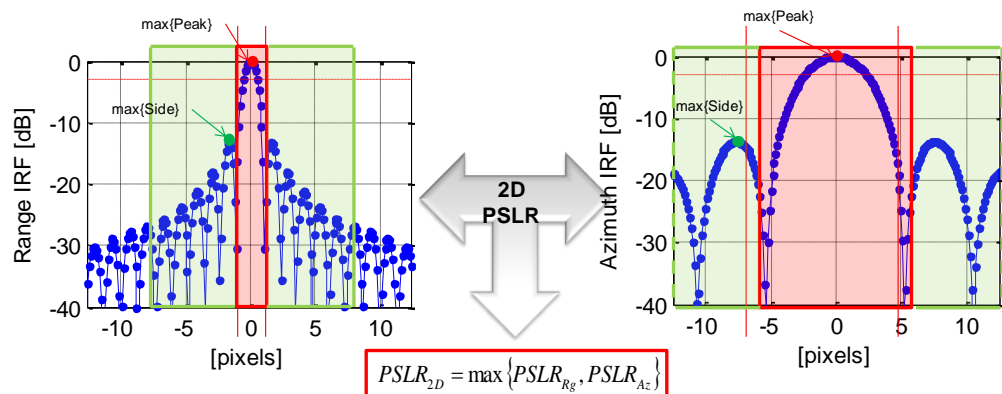


Figure 4-5: Example of Peak to Side Lobe Ratio measurements. The light red area refers to the peak area, the light green area to the side lobes area. The max of the peak and of the side lobes are highlighted. The left-hand panel refers to range, the

right-hand panel to azimuth. The worst case of range and azimuth PSLR is taken as 2D PSLR.

The ISLR is similarly measured from the range and azimuth profiles extracted from the 2D oversampled image. The energy of the main lobe is measured in the area corresponding to two resolution cells around the peak location. The energy of the side lobes is measured in the areas corresponding to 9 resolution cells to the left and to the right of the main lobe.

The mathematical definition of the ISLR is:

$$ISLR_{Rg} = -10 \cdot \log_{10} \left(\frac{\int_{Peak} |S(rg)|^2 drg}{\int_{Side} |S(rg)|^2 drg} \right) \quad (6)$$

$$ISLR_{Az} = -10 \cdot \log_{10} \left(\frac{\int_{Peak} |S(az)|^2 daz}{\int_{Side} |S(az)|^2 daz} \right)$$

ISLR parameter can also be extended to the 2D case, considering the integration over a two-dimensional area of side lobes obtained combining the areas for 1D parameters as reported in **Figure 4-6** where the red area corresponds to the main lobe and the yellow one to the side lobes. The mathematical definition for the 2D ISLR is:

$$ISLR_{2D} = -10 \cdot \log_{10} \left(\frac{\iint_{2DPeak} |S(rg, az)|^2 drgdaz}{\iint_{2DSide} |S(rg, az)|^2 drgdaz} \right) \quad (7)$$

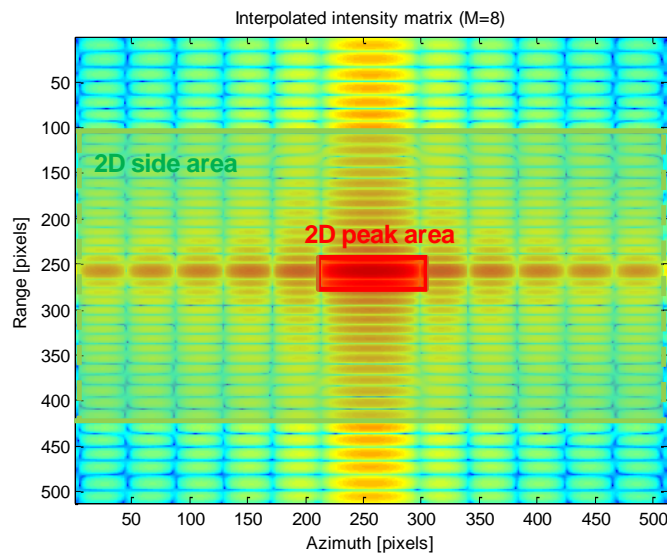


Figure 4-6: 2D IRF of a simulated point target where the 2D peak area and the 2D side area are pointed out

Similarly, to the resolution case, the measured PSLR and ISLR can be compared with the theoretical values from the processing parameters applicable to the product under analysis. Discrepancies between the measured and theoretical values could hint some problems during the processing of the data. For instance, a wrong Doppler Centroid estimation can

lead to an error in the whitening of the azimuth antenna with consequent increase of the side lobe levels.

Finally, it is worth noting that side lobe levels measurement from real data requires a very good SNCR in order to get unbiased estimates particularly in case of heavy Hamming weighting resulting in very low side lobe levels.

4.2.5 Point Targets localization

The possibility to convert from SAR coordinates (azimuth and range times) to geographic coordinates (latitude, longitude and height) and vice versa is fundamental for the interpretation of SAR data.

The conversion is performed basing on the SAR orbit state vectors, representing satellite positions and velocities during the acquisition. The geolocation accuracy of a SAR product represents the accuracy that can be achieved in the conversion from SAR coordinates to geographical coordinates (direct geocoding) and vice versa (inverse geocoding). The geolocation accuracy can be measured from a point target SAR image by comparing the position of the peak of the target in the SAR data with the expected position computed with an inverse geocoding operation from the target ground position and the platform orbit.

The comparison is performed in SAR SLC domain (azimuth and range times domain) according to the following procedure:

1. The accurate position of the target in the SAR data is measured from the 2D oversampled image in order to improve the accuracy of the estimation. The obtained point target coordinates are expressed in fast $t_{rg,meas}$ and slow $t_{az,meas}$ times.
2. The ground position of the point target is converted in SAR coordinates through an inverse geocoding operation. The inverse geocoding is the procedure aimed at finding the azimuth time at which a point on the Earth is imaged by the sensor, given:
 - a. the ground point location \mathbf{P} in the 3D space (Earth Centered Earth Fixed (ECEF));
 - b. the Doppler Centroid (DC) f_{DC} at which the ground point is imaged (if the SAR image under analysis is focused in a Zero Doppler geometry $f_{DC} = 0$).
 - c. the sensor position expressed as a function (polynomial) of the azimuth time $\mathbf{S}(t_{az})$ in the 3D space (ECEF);
 - d. the sensor non-inertial velocity expressed as a function (polynomial) of the azimuth time $\mathbf{V}(t_{az})$ in the 3D space (ECEF);

The actual inverse geocoding procedure is just the solution of the following equation:

$$[\mathbf{P} - \mathbf{S}(t_{az})]\mathbf{V}(t_{az}) - \frac{f_{DC}\lambda}{2}|\mathbf{P} - \mathbf{S}(t_{az})| = 0 \quad (8)$$

where λ is the sensor wavelength. This is a non-linear equation which is solved by exploiting numerical methods (e.g. Newton-Raphson). Once that the azimuth time $t_{az,geo}$ has been retrieved it is straightforward to obtain the sensor position, the sensor velocity and the slant range $t_{rg,geo}$ corresponding to the imaged ground point.

3. The geolocation error is then expressed as the difference between the measured and predicted target position in SAR coordinates

$$\begin{cases} \varepsilon_{rg} = t_{rg,geo} - t_{az,meas} \\ \varepsilon_{az} = t_{az,geo} - t_{az,meas} \end{cases} \quad (9)$$

The measured localization errors in time can then be converted into space by multiplying by half the speed light (range error) and the satellite ground velocity (azimuth error).

The measured geolocation error is expected to be as close to 0 as possible. When discrepancies are observed the main causes can be:

- Orbital information inaccuracy resulting in errors either in range and/or azimuth directions
- Instrument internal delays not properly compensated and introducing errors in the range direction
- Additional propagation delay through troposphere (for all bands) and ionosphere (especially for L and lower bands but possible also for higher bands in case of strong ionosphere). Such delay is usually not compensated at processing level and shall then be compensated in post processing to improve the accuracy of the process.
- Geodynamics effects introducing small shifts in azimuth and range directions. Similar to troposphere and ionosphere, such effects are not compensated at processing level but, only for high resolution data given the small magnitude, can be compensated in post processing.

In case of polarimetric data, the polarimetric co-registration can be performed by measuring the difference in a point target location between two polarization channels.

4.3 Distributed Target Data Analysis

The images with homogeneous distributed targets allow to verify the product quality globally. The main measures that can be performed over distributed data include:

- Radiometric profiles for relative calibration and EAP compensation
- Equivalent number of looks

In particular, low backscatter areas can be exploited for the measurement of:

- Radiometric profiles for NESZ level

4.3.1 Beta/Sigma/Gamma-Zero profiles

The distributed data can be exploited to derive data profiles for the SAR products radiometric calibration assessment. The profiles generation is actually a simple operation requiring to average a certain number of range or azimuth lines. Obtained profiles can then be exploited to verify some data properties such:

- Expected trends with regards to incidence angle (e.g. γ^0 profiles for Rain Forest acquisitions are expected to be incidence angle independent and hence flat)

- NESZ profiles for only noise data (either simulated or acquired over very low back-scatter area)
- Azimuth trends in particular for acquisition modes like TopSAR or SCANSAR

The main processing steps needed for the generation of the radiometric profiles are:

1. Conversion between input and required radar observable. As discussed in **Section 4.1**, according to the processing options applicable to SAR image under analysis, the input data can be provided in one between β^0 , σ^0 or γ^0 quantities. Depending on the desired output quantity the required conversion, according to **Table 4-2** shall be performed before computing the desired profile.
2. The converted input data can then be averaged to generate the output radiometric profiles to be used for the SAR products validation.

The first step mainly consists in the conversion between the original slant range axis of the input SLC data into incidence angle values. This is achieved by computing a set of ground points corresponding to the slant range axis of the data through the direct geocoding operation. The direct geocoding is the procedure used to find the position of a target P in the 3D space, hence its coordinates $P(x_p, y_p, z_p)$ given:

1. the sensor location $S(x_s, y_s, z_s)$ in the 3D space (ECEF);
2. the (azimuth) slow time, t_{az} at which the sensor images the target. The middle of the scene is assumed as reference for this analysis.
3. the target-sensor distance R_s

The direct geocoding procedure consists in the solution of a system of three equations:

$$\begin{cases} |\mathbf{S} - \mathbf{P}| = R_s \\ \mathbf{v}_s \cdot (\mathbf{S} - \mathbf{P}) = 0 \\ \frac{P_x^2 + P_y^2}{R_e^2} + \frac{P_z^2}{R_p^2} = 1 \end{cases} \quad (10)$$

where R_e and R_p are the equatorial and polar radius of the reference ellipsoid.

The three equations correspond to:

- Range equation
- Doppler equation
- Earth ellipsoid model;

The intersection of the range sphere, the Doppler plane and the Earth ellipsoid provides two solutions that correspond to the left and right looking sensors. These solutions are achieved by numeric techniques. In particular the numerical approach known as Newton-Raphson method, is implemented.

The incidence angle corresponding to the ground targets is then retrieved as:

$$\vartheta_{inc} = \cos^{-1} \left(\frac{\mathbf{S} - \mathbf{P}}{\|\mathbf{S} - \mathbf{P}\|} \cdot \frac{\mathbf{P}}{\|\mathbf{P}\|} \right) \quad (11)$$

where \cdot stands for the dot products between the point target Line Of Sight (LOS) and the local normal to the ground surface. An incidence angle for each slant range sample is obtained and the needed radar observable conversion is performed according to the computed incidence angles vector. **Table 4-2** provides a resume of the applied corrections factors. It is worth to mention that correction of the radiometry based on the incidence angle is not the solution with best accuracy (that instead is based on the correction of the local backscatter area [RD-3]). Nevertheless, considering that the assessment is performed over Rain Forest area with reduced topography variation, the accuracy of the two methods is comparable and the correction based on incidence angle is simpler.

Table 4-2 Resume of radar observable conversions

| Input radar observable | Output radar observable | | |
|------------------------|----------------------------------|------------------------|----------------------------------|
| | β^0 | σ^0 | γ^0 |
| β^0 | 1 | $\sin \vartheta_{inc}$ | $\tan \vartheta_{inc}$ |
| σ^0 | $\frac{1}{\sin \vartheta_{inc}}$ | 1 | $\frac{1}{\cos \vartheta_{inc}}$ |
| γ^0 | $\frac{1}{\tan \vartheta_{inc}}$ | $\cos \vartheta_{inc}$ | 1 |

The second step consists in the computation of the radiometric profile by averaging the user selected data portion. In case real data are analyzed, the selection can include inhomogeneities due to the structure of the imaged scene. For such cases it is possible to activate the data masking option. A mask of pixel outliers is generated starting from the statistics of the input data intensity. The pixels masking is performed by analyzing the distribution of neighbor pixels (rectangular window) and discarding the outliers. **Figure 4-7** shows an example of the pixels flagged as invalid (red pixel in the image on the right). The original radar brightness map is represented on the left.

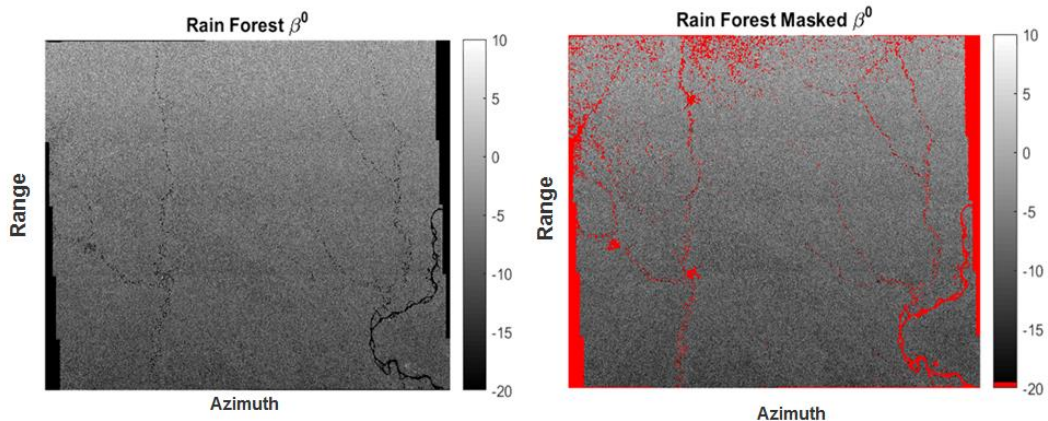


Figure 4-7: Example of Rain Forest data masking. The image on the left is the original product. The image on the right shows the discarded pixels in red.

Figure 4-8 shows an example of the extraction of the range profiles from a Rain Forest product. The original image is in σ^0 . The plot on the left has been obtained requiring no radar observable conversion. The plot on the right has been obtained requiring the output profiles in γ^0 . The two lines represent the co (red) and cross (green) polarization channels. The result of the conversion is that γ^0 profiles show a slightly higher value (the acquisition incidence angle is around 20 degrees corresponding to a radiometric gain of +0.3 dB) and do not show the slight decreasing trend of the σ^0 profiles (as expected).

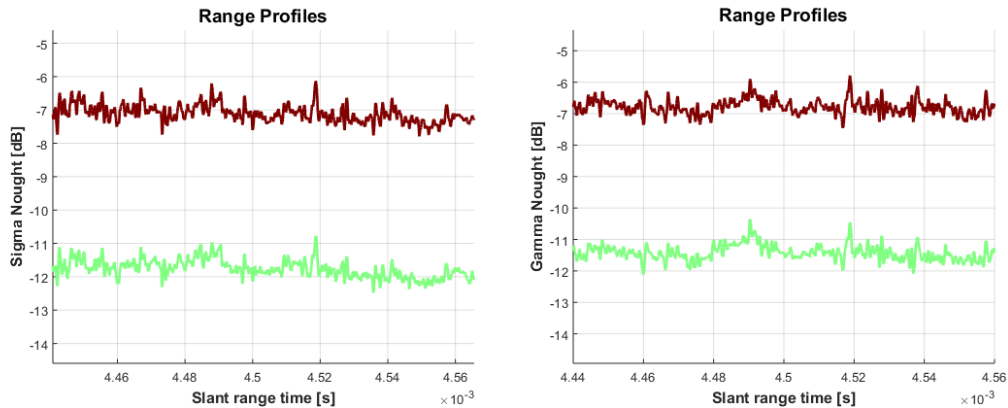


Figure 4-8: (Left) Original σ^0 range profile of the analysed product. (Right) Converted γ^0 range profile of the analysed product

4.3.2 Beam-to-beam calibration and EAP compensation

The γ^0 profiles obtained as described in the section above can be finally exploited to assess relative radiometric calibration in case of ScanSAR and TopSAR modes by comparing the average γ^0 levels from beam to beam.

Moreover, comparing the γ^0 profiles with the antenna pattern allows the estimation of the residual roll correction. **Figure 4-9** shows an example of the results of the γ^0 profiles estimation from a product acquired over the rain forest. The colour represents the number of points falling in a certain bin. The dashed black line is the estimated average γ^0 profile. The obtained profile is very flat showing a nice agreement between predicted and actual EAP.

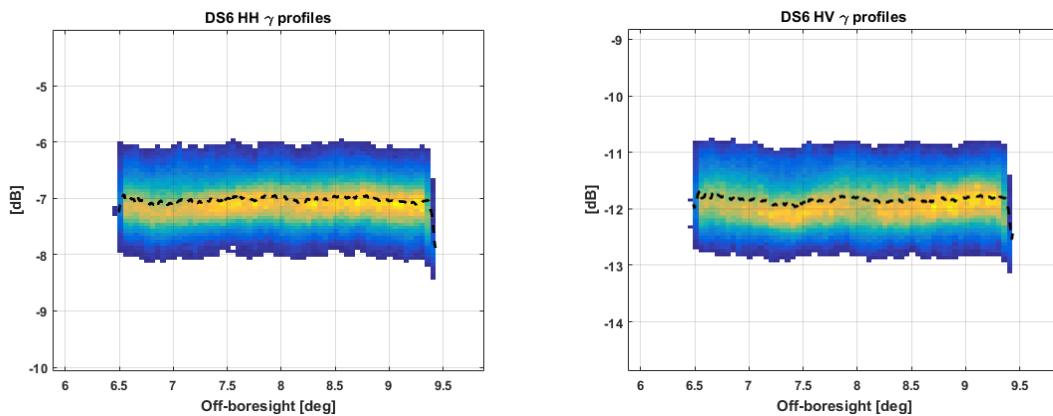


Figure 4-9: Example of results of γ^0 profiles extraction from an acquisition over Congo Rain Forest. The colour represents the number of points falling in a certain bin. The dashed black line is the estimated average γ^0 profile.

4.3.3 Azimuth scalloping

A further analysis which can be performed on ScanSAR and TopSAR data acquired over rain forest is the derivation of the residual scalloping profile. Scalloping is a characteristic of ScanSAR images due to the azimuth elementary pattern of each TRM introducing an

additional gain factor on the squinted beams. This gain is compensated during the processing exploiting a model of the azimuth elementary pattern. After scalloping compensation, each burst is expected to be flat in the azimuth direction.

The derivation of the residual scalloping profile is performed at the same time of the γ^0 -profile estimation and the processing is very similar. For the residual scalloping profile estimation, the average data level is removed since the overall beam gain is already accounted for in the γ^0 -profile analysis. **Figure 4-10** shows the results of the residual scalloping profile estimation for two different beams in a ScanSAR acquisition. The colour is proportional to the points density considering that all the bursts of the acquisition have been analysed. The dashed black line is the average residual profile. In both cases it can be noticed that the residual scalloping profile is included in the range ± 0.1 dB and is not completely flat.

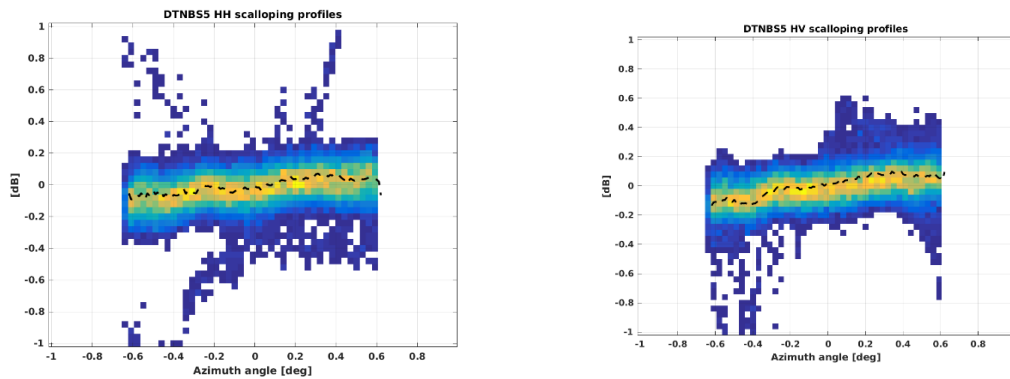


Figure 4-10: Example of residual scalloping profiles for two beams of a ScanSAR acquisition, as a function of the steering angle. The colour is proportional to the points density. The dashed black line is the average residual profile.

4.3.4 NESZ level

The σ^0 profiles obtained as described in **Section 4.3.1** can be exploited to assess the NESZ. The NESZ level thus obtained from SLC data can then be compared with the NESZ maps if generated by the processor or, in general, with the expected level.

The NESZ level estimation is typically performed for cross-pol channels only since signal level in co-pol channels is always too high. The performed processing is pictorially recalled in **Figure 4-11** and is quite simple.

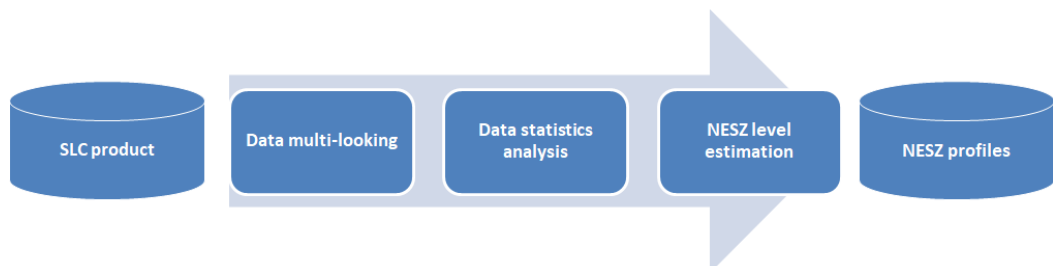


Figure 4-11: Flow chart for NESZ level estimation

The data are divided into blocks of 2000 azimuth lines to cope with the natural variability of the observed scene (even patches of calm ocean are usually not too big). Firstly, a multi-looking operation is performed to enhance the radiometric resolution of the noise level estimation process. The operation is performed through a boxcar window in time domain. The selection of the window size is a trade-off between the need of a large window to enhance radiometric resolution and the need of a small window to avoid including backscatter variations in the analysis.

As an example, **Figure 4-12** shows the quick look of the cross pol channel of an acquisition over Doldrums, in which it is possible to identify some regions where backscatter is particularly low, and in **Figure 4-13** the central portion (10000 azimuth lines) of the same acquisition is plotted before (left) and after (right) multi-look: as expected the radiometric resolution of the image on the right is improved.



Figure 4-12: Quick look of the cross-pol channel of an acquisition over Doldrums

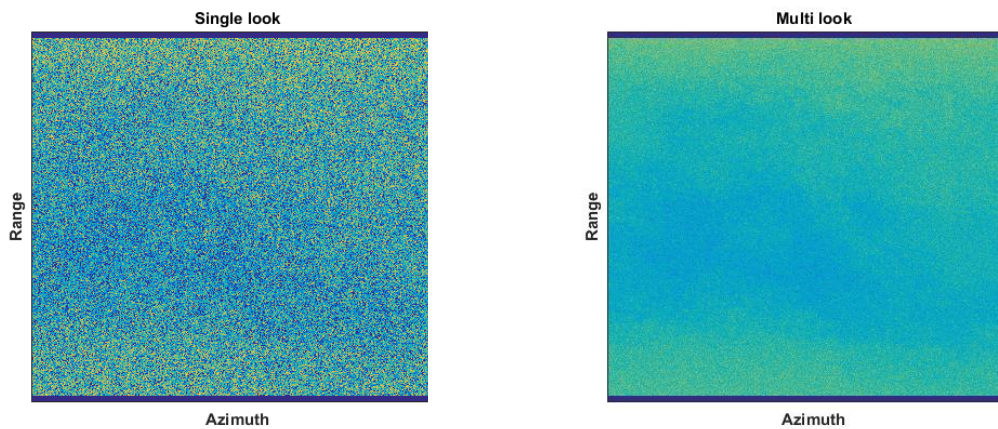


Figure 4-13: Central portion of the cross-pol channel of an acquisition over Doldrums. (Left) Single look and (right) multi looked.

The second step is the statistical analysis of the filtered block of data to identify for each range line the most likely NESZ level. The range-by-range processing is necessary due to the fact that the radiometric corrections applied by the processor make the noise level variable in range. The processing consists in the identification of a given percentile to be associated to the NESZ level in the data. The percentile selection is dependent on the considered multi looking window (the larger the window the lower the percentile). Ideally, for a very large window, the NESZ level would be associated to the minimum backscatter value measured in the range line.

Figure 4-14 provides an example of the σ^0 distribution for three blocks of data located at near (blue), mid (red) and far (yellow) range of the data portion shown in **Figure 4-13** (multi looked). All the values are very close to the expected NESZ level but some signal is still clearly present.

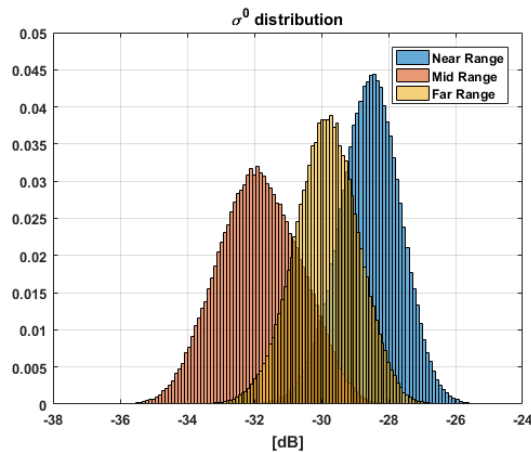


Figure 4-14: σ^0 distribution for three blocks of data located at near (blue), mid (red) and far (yellow) range of an acquisition over Doldrums

In the end, a NESZ profile for each analysed data block is obtained. **Figure 4-15** shows the NESZ profiles obtained from the analysis of the example acquisition. A total of 31 profiles are reported on the left. The image on the right represents the 2D distribution of the profiles. The black line is the average noise vector from the NESZ map generated by the processor. Considering that some signal is clearly present in the data, the agreement with the NESZ profile is quite good in particular at near range where the estimated NESZ curve is very close to the black line.

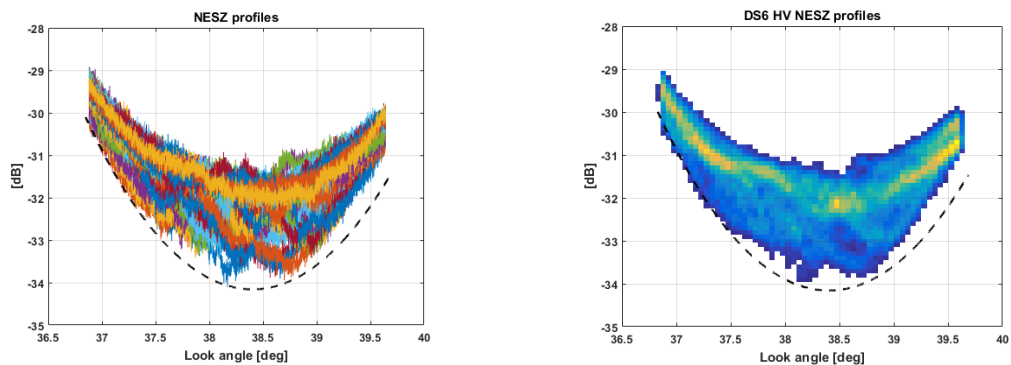


Figure 4-15: NESZ profiles obtained from the analysis of an acquisition over Doldrums. (Left) Plot of each individual profile and (right) 2D distribution of the profiles. The black line represents the average noise vector from the NESZ map generated by the processor.

4.3.5 Equivalent Number of Looks (ENL)

SAR data are complex random variable whose distribution in case of homogeneous distributed target can be assumed as circular Gaussian. The resulting intensity probability distribution is the gamma distribution. An accurate estimation of the backscatter requires that several independent SAR samples are averaged together to reduce speckle noise. Such operation is called multi-looking and the intensity probability distribution of a multi-looked images tends to a Gaussian at the increase of the number of looks.

The ENL is a quality parameter that can be estimated from SAR data to measure the “level” of multi-looking of the analyzed product. It is a statistical measure of how many

independent pixels have been measured to generate the SAR image. The ENL parameter is computed from a block of SAR data as:

$$ENL = \frac{E\{I\}^2}{\text{var}\{I\}} \quad (12)$$

where E is the average operator, var stands for the variance and I is the considered pixels intensity.

If SLC images are analyzed, the expected result of ENL estimation is 1. The actual result is usually lower than 1 since the sampling of the data is always slightly higher than the resolution, meaning that the image pixels are not totally independent. Also, it is important that the portion of data selected for the analysis is homogeneous, otherwise the assumptions on data statistics are no longer valid.

Figure 4-16 shows an example of ENL estimation over a SLC image acquired over Rain Forest. The estimation over the data portion shown in the top plot is biased by the presence of the river and gives an ENL measure of 0.72. The data portion in the bottom plot is much more homogeneous and gives an ENL measure of 0.84, closer to the theoretical limit of 1.

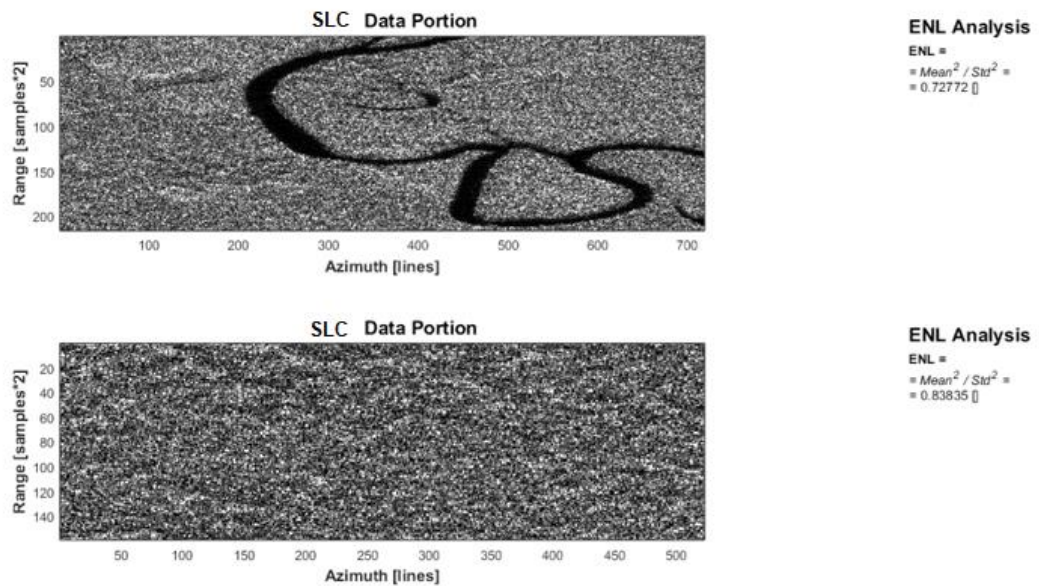


Figure 4-16: ENL estimation from a block of Rain Forest data. (Top) Non-homogeneous data case. (Bottom) Homogeneous data case.



[END OF DOCUMENT]